Basicity and Porosity of a Calcined Hydrotalcite-Type Material from Nitrogen Porosimetry and Adsorption Microcalorimetry Methods

M. L. Occelli,*,† J. P. Olivier,‡ A. Auroux,§ M. Kalwei,|| and H. Eckert||

MLO Consulting, 6105 Black Water Trail, Atlanta, Georgia 30328, Micromeritics Instrument Corp. Inc., Norcross, Georgia 30093, Institut de Recherches sur la Catalyse, CNRS, 2 Av. A. Einstein, 69626 Villeurbanne, France, and Institut fur Physikalische Chemie Westfälische Wilhelms Universität Münster, Schlossplatz 7, D 48149, Münster, Germany

Received April 28, 2003. Revised Manuscript Received July 7, 2003

The hydrothermal transformation at 90−95 °C of a slurry of Al_2O_3/MgO/(CH_3COOH)/H_2O with molar oxide composition 1:4.4:2.2:1111 produced a hydrotalcite-like (HT) material free from phase impurities and having an approximate unit cell composition of $Mg_{0.66}Al_{0.33}(OH)_2(CHCOO)_{0.33}$. ^{13}C NMR and ^{27}Al NMR spectra have revealed that the air-dried solid contains acetate anions probably as charge-compensating anions in the HT interlamellar space and that all the aluminum is present in octahedral coordination. After calcination in air at 500 °C, the stacks of brucite layers that form the HT crystals exfoliate, forming a stable mesoporous "house-of-cards" structure with pore width in the range 2.5−20.0 nm, characterized by a DFT surface area of 254 m^2/g and total pore volume of 0.33 cm^3/g at 0.995 *p*/Po, that is available to sorption and catalysis. A 5-h exposure to 100% steam at 760 °C collapses the HT material forming a residue that contains a well-crystallized MgO and an Al spinel phase identified by XRD. At 30 °C, adsorption microcalorimetry with SO_2 revealed that the calcined HT material behaves like a solid base possessing a large (530 μmol SO_2/g) population of basic sites with strength near 170 kJ/mol; the strength of the strongest basic site is 190 kJ/mol. The steam-aged HT retains the strength of its strongest basic sites but loses most of its sorption capacity for SO_2. Thus, materials of this type should be efficient adsorbents for the removal of sulfur oxides and other acidic air pollutants in industrial applications that do not require the abovementioned hydrothermal stability.

Introduction

Hydrotalcite is a naturally occurring mineral[1−3] with typical composition $Mg_6Al_2(OH)_{16}CO_3{\cdot}4H_2O$ consisting of stacks of brucite-like layers in which Mg(VI) atoms are replaced in part by Al(VI) atoms, thus generating sheets having a net positive charge that is compensated by interlamellar anions. Although, in principle, any anion could be placed in the interlamellar space, carbonates are the anions commonly found in naturally occurring materials. Hydrotalcite-like compounds are layered double hydroxides (LDHs) with the general formula: $[M^{II}_{1-x}M^{III}_x(OH)_2\ ]^{x+}A^{z-}_{x/z}{\cdot}nH_2O$ where M^{II} is a divalent cation (such as Mg, Ca, Mn, Fe, Co, Cu, Zn, and Ni) and M^{III} is a trivalent cations (such as Al, Cr, Mn, Co, Ni, La, and Fe) and A is the charge compensating anion.[3,4] Divalent and trivalent cations are randomly distributed in the brucite-like layer; the charge of LDHs is controlled by the degree of isomorphous substitution of M^{II} by M^{III} cations while the charge density distribution is controlled by the distribution of M^{III} ions in the octahedral layers.[5] A unique characteristic of these layered materials is their ability to reconstruct their layered structure, lost on heating at a temperature not exceeding 400 °C, when exposed to the desorbed solvent; this property is lost at 500 °C.[4]

In contrast to smectites,[6] hydrotalcites and synthetic hydrotalcite-like materials are referred to as anionic clays owing to their ability to exchange charge-compensating interlamellar anions with a variety of organic and inorganic anions.[4] As a result, it is possible to generate LDHs with a variety of properties. Of particular interest is the reported use of LDHs in the preparation of fluid cracking catalysts (FCCs) for the conversion of sulfur-containing feedstocks.[7] A detailed review of the synthesis, characterization, and physicochemical characteristics of LDHs is in ref 4.

* To whom correspondence should be addressed. Phone: 404-303-7958. E-mail: mloccell@mindspring.com.
† MLO Consulting.
‡ Micromeritics Instrument Corp. Inc.
§ Institut de Recherches sur la Catalyse.
|| Universität Münster.

(1) Frondel, C. *Am. Miner. Magn.* **1941**, *26*, 295−315.
(2) Taylor, H. F. W. *Miner. Mag.* **1973**, *39*, 377−389.
(3) Allmann, R. *Acta Crystallogr., B* **1968**, *24*, 972.
(4) Cavani, F.; Trifiro, F.; Vaccari, A. *Catal. Today* **1991**, *11*, 173−301.
(5) De Roy, A.; Forano, C.; El Malki, K.; Besse, J−P. In *Synthesis of Microporous Materials. II: Expanded Clays and Other Microporous Solids*; Occelli, M. L., Robson, H., Eds.; Van Nostrand Reinhold: New York, 1992; p 108.
(6) Grim, R. E. *Clay Mineralogy*; McGraw-Hill: New York, 1968.
(7) van Broekhoven, E. H. U.S. Patents 4,866,019, 1989; 4,946,581, 1990; 4,952,382, 1990.

10.1021/cm030105b CCC: $25.00
Published on Web 10/04/2003

It is the purpose of this paper to report our examination of the porous structure and basic properties of a synthetic hydrotalcite-like sample after calcination in air at 500 °C and after 5 h of steam-aging at 760 °C with 100% steam to simulate the aging of FCCs at microactivity test conditions.

Experimental Section

Materials Preparation. A hydrogel of composition Al_2O_3/$(CH_3COOH)/H_2O$ (0.1:0.22:27.8) was prepared by slurring pseudobohemite (Catapal B) in a diluted acetic acid solution according to a published procedure.[8] After heating the hydrogel (with stirring) at 60 °C for 1 h, a second slurry of MgO/H_2O (0.44:83.3) prepared by suspending MgO (99.95%, −325 mesh powder from Alfa) in water, was added to the hydrogel, and the resulting mixture was heated at 90−95 °C overnight (with stirring) in a round-bottom flask equipped with condenser and stirring mechanism. This procedure has been described in detail elsewhere.[9] The solid was recovered by filtration under vacuum, washed with an excess of hot (60 °C) DI water, and then allowed to dry at 25 °C in a desiccator overnight. The pristine material was then calcined in flowing air at 500 °C (calcined sample) and exposed for 5 h to 100% steam at 760 °C (steam-aged sample). Thermogravimetric analysis was performed with a TG-DSC 111 Setaram instrument using a heating rate of 5 °C/min and 0.42 cm^3/s of an air/He mixture as a purge gas. X-ray powder diffraction (XRD) spectra were obtained with Cu Kα radiation using a Philips PW 3710/3020 diffractometer equipped with a monochromator. The measurements were made using a step scanning program with 0.02° per step and acquisition time of 5 s per step.

Nitrogen Porosimetry. Nitrogen sorption isotherms obtained at liquid nitrogen temperature were collected over a wide pressure range using a volumetric technique on a Micromeritics ASAP 2010 adsorption instrument. Prior to analysis, samples weighing from 0.1 to 0.3 g were outgassed in a vacuum at 250 °C for at least 16 h; for the air-dried HT sample degassing was performed at 100 °C to avoid decomposition of acetate anions. The total pore volume (PV) was derived from the amount of nitrogen adsorbed at a relative pressure close to unity ($p/P_o = 0.995$) by assuming that all the accessible pores were then filled with liquid nitrogen; p is the equilibrium pressure and Po is the saturated vapor pressure of the adsorptive at the temperature of the experiment. Surface area (SA) measurements were performed using the Brunauer−Emmett−Teller (BET),[10] Langmuir,[11] and Barret−Joyner−Halenda (BJH) equations[12] and compared with results obtained with DFT methods.[13,14] DFT data refer to cylindrical pore widths equal to or less than 33.4 nm. The total surface areas reported in Tables 1−3 include the areas of unfilled pores larger than 33.4 nm, which is given by the DFT analysis.

Solid State NMR. ^{27}Al MAS NMR spectra were obtained at 130.2 MHz, using a Bruker Avance (DSX) 500 spectrometer. Samples were spun in cylindrical 4-mm zirconia rotors at a spinning frequency of 12 kHz. The spectra were recorded with short pulses of 2 μs (flip angle <45°) and relaxation delays of 1 s. Resonance shifts are reported using liquid samples of 1 M aqueous solutions of $Al(NO_3)_3$ as external reference standard. Because the exact spectral parameters of the Al(IV) and Al(VI) signal components are not exactly known (due to a distribution of quadrupolar coupling parameters) no ^{27}Al line shape deconvolution was attempted.

^{13}C−CP-MAS NMR were recorded at 50.3 MHz on a Bruker CXP-200 spectrometer equipped with a 7-mm CP/MAS double resonance probe operated at a rotation frequency of 2 kHz. The chemical shifts are reported relative to liquid tetramethylsilane, using a sample of solid adamantane ($\delta_{CH} = 38.6$ ppm) as secondary standard.

Microcalorimetry. Heat of adsorption of SO_2 was measured using a heat-flow microcalorimeter of the Tian−Calvet type (from Setaram) linked to a glass volumetric line. Successive doses of gas were sent onto the sample until a final equilibrium pressure of 133 Pa was obtained. The equilibrium pressure relative to each adsorbed amount was measured by means of a differential pressure gauge from Datametrics. The adsorption temperature was maintained at 30 °C. Primary and secondary isotherms were collected at these temperatures. To avoid decomposition of interlamellar acetate anions, the air-dried HT sample was activated in a vacuum at 150 °C, while the calcined and steamed samples were activated overnight under vacuum at 500 °C, before calorimetric measurements were undertaken; SO_2 chemisorption data are in Tables 4 and 5.

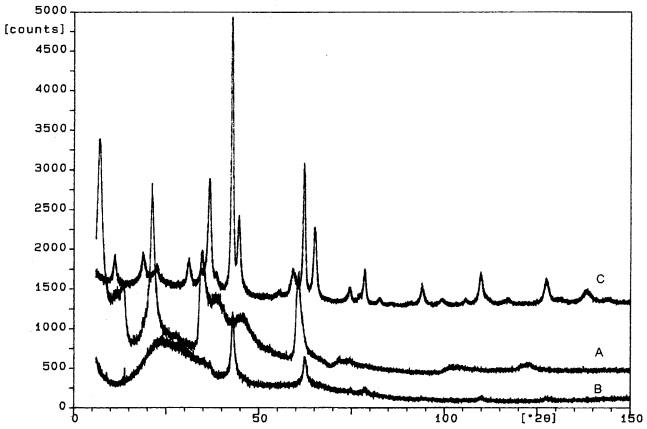

Figure 1. X-ray diffractograms for (A) HT crystals at 25 C; (B) HT crystal after calcination in air at 500 °C; and (C) HT crystals after steam aging (760 °C, with 100% steam).

Results and Discussion

The hydrothermal transformation at 90−95 °C/10 h of a slurry of $Al_2O_3/MgO/(CH_3COOH)/H_2O$ with molar oxide composition 1:4.4:2.2:1110 produced a hydrotalcite-like material essentially free from phase impurities such as unreacted MgO or Al_2O_3, Figure 1 (middle). This solid was found to contain small amounts of Ca and Na (0.4% CaO and 1.0% Na_2O) probably associated with impurities in the reactants used. Elemental analysis of the reaction product gave Mg/Al = 2.1 and Al/$[CH_3COO] = 1.02$ consistent with an approximate unit cell composition of $Mg_{0.66}Al_{0.33}(OH)_2(CHCOO)_{0.33}$ in agreement with published results[8] and indicating that the aforementioned hydrothermal reaction is almost stoichiometric. The powder XRD pattern in Figure 1 (bottom) shows that the hydrotalcite structure disappears upon heating the solid in air at 500 °C/4 h (or at 640 °C/1 h); the two broad and weak lines at $2\theta =$ 43.0° and 62.3° are consistent with the presence of MgO. Interestingly, after cooling the sample to room temperature in air from 500 °C, the weight increased by 20% revealing the desiccant property of the calcined material. Steam aging (760 °C/5 h with 100% steam)

(8) Kelkar, C. P.; Schutz, A. A.; Cullo, L. A. In *Synthesis of Porous Materials*; Occelli, M. L., Kessler, H., Eds.; Marcel Dekker: New York, 1996; pp 691−703.

(9) Schutz, A. A.; Cullo, L. A.; Kelkar, C. P. U.S. Patent 5,399,329, 1995.

(10) Brunauer, S.; Emmett, P. H.; Teller, E. *J. Am. Chem. Soc.* **1938**, *60*, 309.

(11) Langmuir, I. *J. Am. Chem. Soc.* **1916**, *38*, 2267.

(12) Barret, E. P.; Joyner, L. S.; Halenda, P. P. *J. Am. Chem. Soc.* **1951**, *73*, 373−380.

(13) Olivier, J. P. In *Surfaces of Nanoparticles and Porous Materials*; Schwartz, J. A., Contescu, C. I., Eds.; Marcel-Dekker: New York, 1999; pp 295−318.

(14) Olivier; J. P.; Koch, S.; Jaroniec, M.; Kruk, M. In *Characterization of Porous Solids V*; Unger, K. K., et al., Eds.; Studies in Surface Science no. 128; Elsevier: Amsterdam, 2000; p 71.

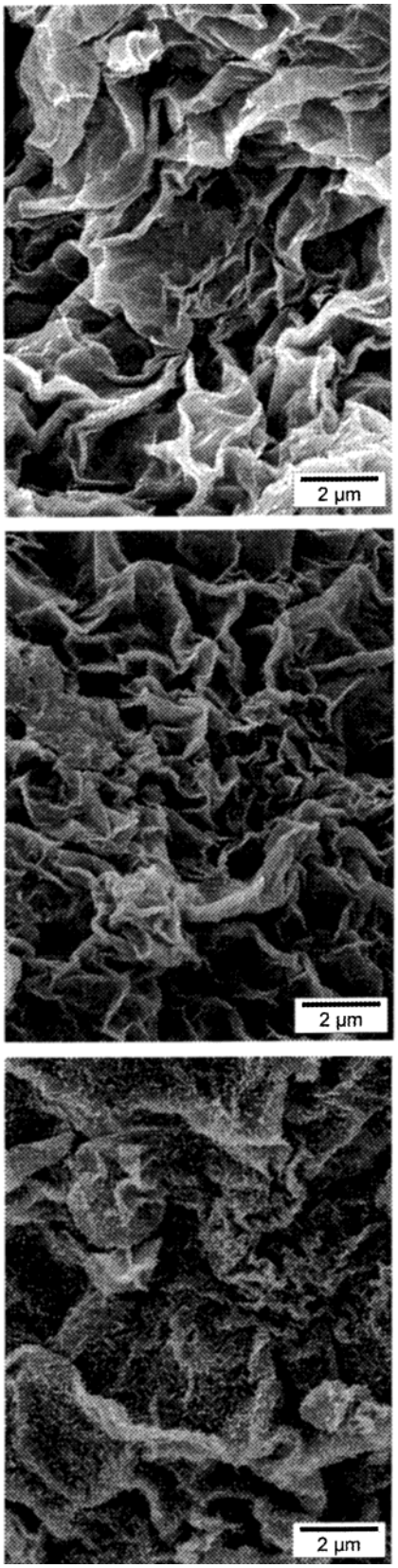

Figure 2. Scanning electron micrographs of the synthetic HT-like material after air drying at 25 °C (top), calcination at 500 °C (middle), and steam aging at 760 °C with 100% steam. (bottom).

produces a well-crystallized spinel, $MgAl_2O_4$[15] together with some MgO[16]; see Figure 1 (top). The weak lines near $2\theta = 11.3°$, 22.8°, 34.7°, and 39.1° in Figure 1 (top) are consistent with the presence of minor amounts of magnesium aluminum hydroxide hydrate.[17] Micrometer-scale scanning electron micrographs (SEM) show that the air-dried HT sample is initially composed of a loose agglomeration of wavy sheets irregular in size and shape, Figure 2(top). The sample surface topography does not change appreciably after calcination at 500 °C, Figure 2 (middle). However, after steam-aging it is possible to observe the formation of rigid and flat plates covered by a second phase having a needlelike appearance, Figure 2 (bottom).

Thermogravimetric Analysis. Thermograms in Figure 3 indicate that the sample under study maintains a constant weight up to 50 °C, and then an evolution of weakly bonded water begins that is completed at 260 °C. Near this temperature the interlayered acetate anions start to decompose, and in the 260−450 °C temperature range, the DTG profile shows the existence of a broad endotherm with a peak minimum near 300 °C and a weak shoulder near 360 °C associated with the decomposition and thermal desorption of acetate fragments in the interlamellar space. When heating is repeated in helium (not shown) instead of air, the thermograms (TG and DTG) obtained are indistinguishable.

The Density Functional Theory. Several adsorption theories are available to extract SA and PV information from experimental adsorption isotherms. The Langmuir and BET formalisms are based on the model of adsorption on a free surface. The Langmuir model assumes the surface saturates after the first adsorbed layer, whereas the BET model presumes that multilayers can form at higher pressures. However, neither model allows for the filling of micropores. Surface areas derived from these two models will differ from the actual area in a way that depends on the solid microporous structure. In contrast, the density functional theory approach treats experimental isotherms as the summation of sorbate uptake, at a given pressure, in pores of variable size H. As a result, the integral equation of isothermal adsorption for the case of distributed pore sizes can be written as the convolution[13]

$$Q(p) = \int dH q(p,H) f(H) \qquad (1)$$

where $Q(p)$ is the total quantity of adsorbate per gram of adsorbent at pressure p in pores H distributed over the entire micro−meso−macro range; $q(p,H)$, the kernel function, describes the adsorption isotherm for an ideally homoporous material characterized by pore width H as quantity of adsorbate per square meter of pore surface, and $f(H)$ is the desired pore surface area distribution function with respect to H.[14] Because we are only interested in the numerical values of $f(H)$, we can rewrite eq 1 as a summation

$$Q(\mathbf{p}) = \sum_{\mathbf{i}} \mathbf{q}(\mathbf{p},H_i)\mathbf{f}(H_i)$$

$$\text{or in matrix notation } \mathbf{Q} = \mathbf{qf} \qquad (2)$$

where $Q(\mathbf{p})$ is an experimental adsorption isotherm interpolated onto a vector $\mathbf{p}$ of pressure points; $\mathbf{q}(\mathbf{p},H_i)$

(15) Sawada, H. *Mater. Res. Bull.* **1995**, *30*, 341.

(16) Cohen, R. E.; Gong, Z. *Phys. Rev. B: Condens. Matter* **1994**, *50*, 12301.

(17) Mascolo, M. *Miner. Mag.* **1980**, *43*, 619.

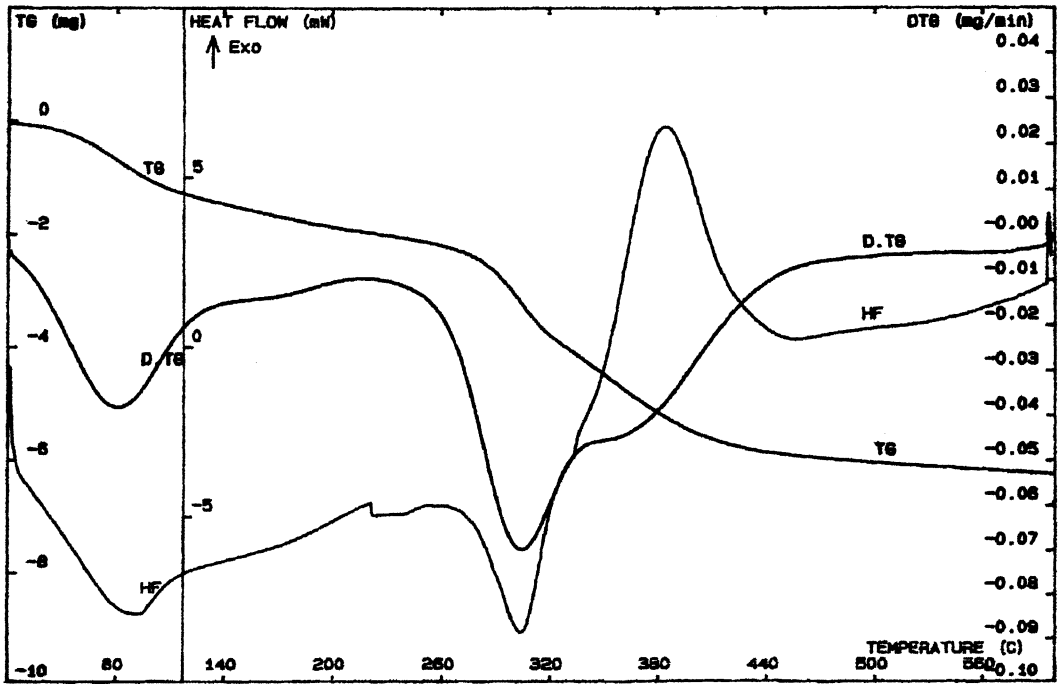

Figure 3. Thermogravimetric (TG), differential thermogravimetric (DTG), and heat flow (HF) profiles of the synthetic HT-like material.

is a matrix of values for quantity adsorbed per square meter, each row calculated for a value of H at pressures **p**, and **f**(H_i) is the solution vector whose terms represent the area of surface in the sample characterized by each pore width H_i. Using the set of hybrid models constructed as described elsewhere[13,14] as the function **q**(**p**,H_i) and the experimental adsorption isotherm for the function Q(**p**), eq 2 can be solved for the distribution vector **f**(H_i). The resulting distributions of pore area and pore volume as a function of pore width are shown later in Figures 7−9.

In addition to pore area and pore volume distributions, adsorption isotherms can provide information on the energetic heterogeneity of surfaces.[13] In fact the integral equation of adsorption can be rewritten as

$$Q(p) = \int d\epsilon \cdot q(p,\epsilon) f(\epsilon) \qquad (3)$$

where $Q(p)$ has the same meaning as in eq 1; $q(p,\epsilon)$ is the local isotherm used to describe the sorbate uptake (per unit area) on a homotattic surface[18] having interaction energy ϵ, and $f(\epsilon)$ is a function that represents the distribution of surface area with energy ϵ. DFT is used to calculate values of $q(p,\epsilon)$, and together with the use of the proper numerical methods, model isotherms thus generated can be used to invert the discretized form of the integral equation of adsorption and obtain the adsorptive potential distribution of the adsorbent from experimental adsorption isotherms; details of this procedure can be found elsewhere.[13] Results are in Figure 4.

Nitrogen Porosimetry Results. As anticipated, the pristine HT sample dried at 25 °C in air has a low DFT surface area of 17 m^2/g and it is essentially void of measurable microporosity because the interlayered space is occupied by charge-compensating acetate anions. The small pore volume of 0.024 cm^3/g reported in Table 1 is attributed to voids between stacks of brucite layers. As a result, adsorption isotherms for a nonporous material of this type can provide information on the surface adsorptive energies. Distribution of adsorptive energy plots could help in the identification of surface debris, variation in chemical composition, and structural

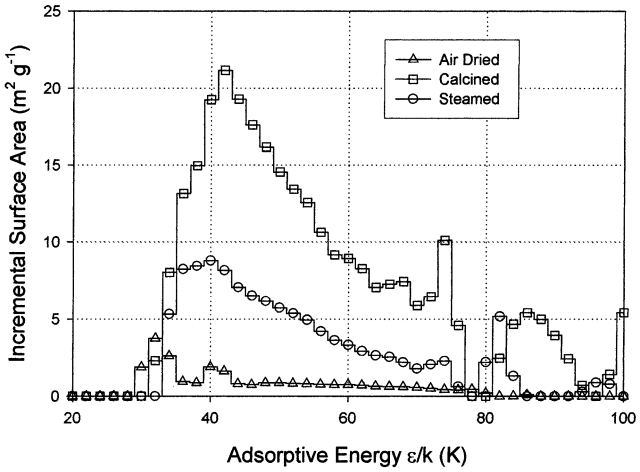

Figure 4. Distribution of ϵ/k on the incremental SA for HT crystals from the experimental nitrogen sorption isotherm at 77 K.

Table 1. Surface Area and Pore Volume Results from Nitrogen Porosimetry Data FOR the Pristine HT Sample Dried in Vacuum at 80 °C[a]

method	micro. surface area (m^2/g)	total surface area (m^2/g)	micro. pore volume (cm^3/g)	pore volume (33.4 nm) (cm^3/g)
DFT	0.0	17	0.0	0.024
BET		22		
Langmuir		14		
BJH		17		0.019

[a] Total PV measured at p/Po ~0.995 = 0.027.

(18) Sanford, C.; Ross, S. *J. Phys. Chem.* **1954**, *58*, 288.

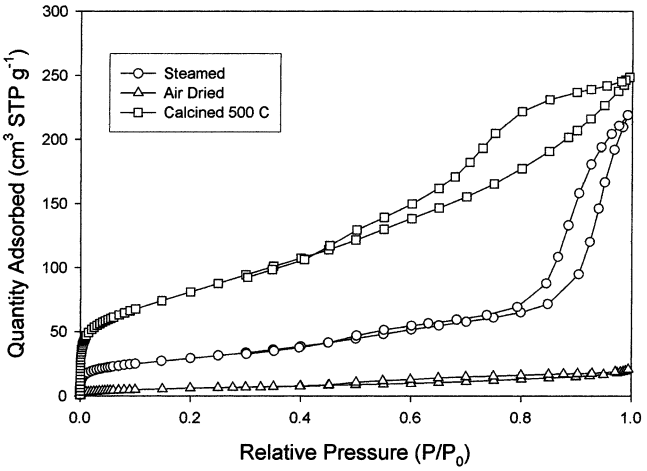

Figure 5. Nitrogen sorption isotherms at 77 K in the high-pressure range.

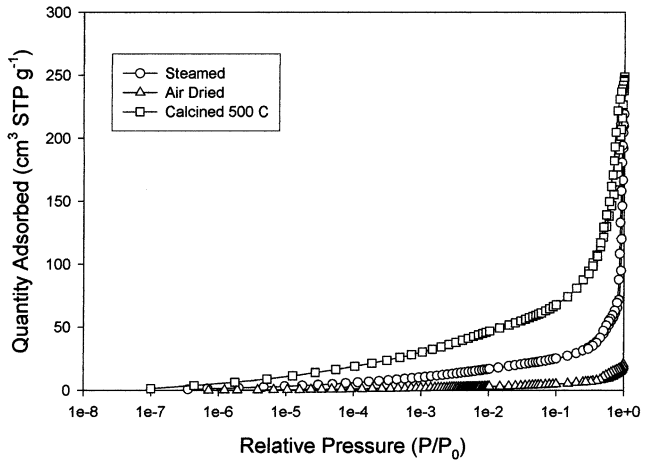

Figure 6. Nitrogen sorption isotherms at 77 K in the low-pressure range.

defects of the HT surface. Plots of surface energy distribution in Figure 4 (bottom) show that the degree of heterogeneity of the pristine, air-dried, HT surface is not high. Surface area with $\epsilon/k = 33$ K is assigned to the oxygens of the brucite layer. After thermal and hydrothermal treatment, the degree of heterogeneity of the HT increases, probably the result of the dehydroxylation of the brucite layers and formation of an Al spinel and MgO mixture; see Figure 4 (top and middle). Surface area with an average ϵ/k of 42 K in Figure 4 is assigned to the oxygens of the dehydroxylated brucite layers. Higher energy areas having ϵ/k =74 K and 80−95 K are attributed to sorption of nitrogen molecules in cavities resulting from the agglomeration of clay platelet aggregates and to quadrupolar interactions of nitrogen with charged sites, respectively. In Figure 4, ϵ is the Lennard−Jones interaction potential of the adsorptive with the surface and k is Boltzmann's constant; ϵ/k has unit of degree Kelvin and is related to the isosteric heat of adsorption.[13] The corresponding sorption isotherms are in Figures 5 and 6.

After removing the acetate anions by heating in air at 500 °C/4 h, the clay total DFT SA increases to 254 m^2/g from 17 m^2/g (Table 2). The isotherm in Figure 5 for the calcined HT closely resembles a type II isotherm; nitrogen uptake monotonically increases with p/Po values due to sorption in the HT mesopores. The same

Table 2. Surface Area and Pore Volume Results from Nitrogen Porosimetry Data for the Calcined (500 °C/2 h in Air) HT Sample[a]

method	micro. surface area (m^2/g)	total surface area (m^2/g)	micro. pore volume (cm^3/g)	pore volume (33.4 nm) (cm^3/g)
DFT	33	254	0.0058	0.18
BET		293		
Langmuir		239		
BJH		241		0.26

[a] Total PV measured at p/Po ~0.995 = 0.33.

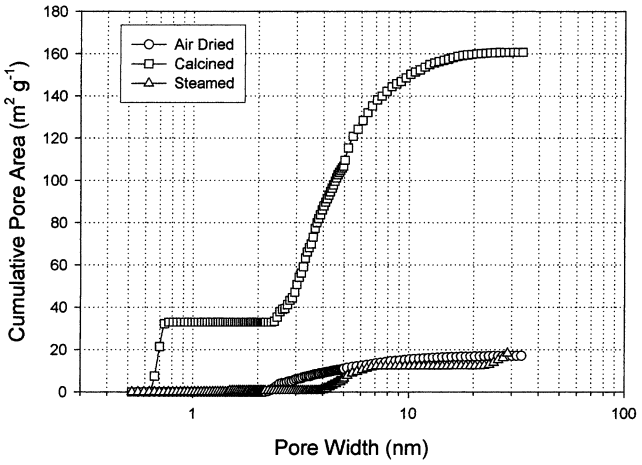

Figure 7. Cumulative pore area distribution data obtained by fitting the DFT model to the sorption isotherms.

data are plotted on a semilog scale in Figure 6. It is shown that even in the very low pressure region near 10^{-7} p/Po nitrogen sorption occurs, although below a relative pressure of 10^{-1} the uptakes of nitrogen are low, a result that can be attributed to the few small mesopores present. Above 10^{-1} p/Po sorption in the sample's larger mesopores cause the rapid uptake of nitrogen seen in Figure 6. The cumulative pore area data are in Figure 7. The calcined sample contains a very small amount of micropores with pore width smaller than 0.75 nm. In the 0.75−2.4 nm range the cumulative pore area remains unchanged and starts to increase again for pore width larger than 2.4 nm. The change in the cumulative pore volume is plotted as a function of pore width in Figure 8. The calcination in air of the HT sample produces a mesoporous residue where the pore volume is mainly contained in pore widths larger than 2.4 nm. At 33 nm the cumulative pore volume is 0.18 cm^3/g. The differential PV vs pore width profile in Figure 9 is clearly asymmetric with peak maximum near 3.7 nm owing to the predominant presence of pore width in the 3.0−6.0 nm range. Thus, results in Figures 7−9 collectively indicate that a distinguishing feature of this porous solid is the presence of negligible amounts of surface area and pore volume in the microspace region.

In Tables 1−3, DFT results are compared to those of traditional methods. In contrast to DFT results reported for solids containing both micro- and mesoporosity,[19−21]

(19) Occelli, M. L.; Olivier, J.; Petre, A.; Auroux, A. *J. Phys. Chem. B* **2003**, *107* (17), 4128−4136.
(20) Occelli, M. L.; Olivier, J.; Auroux, A. *Langmuir* **2002**, *25*, 9816−9823.
(21) Occelli, M. L.; Olivier, J. P.; Auroux, A. *J. Catal.* **2002**, *209*, 385−393.

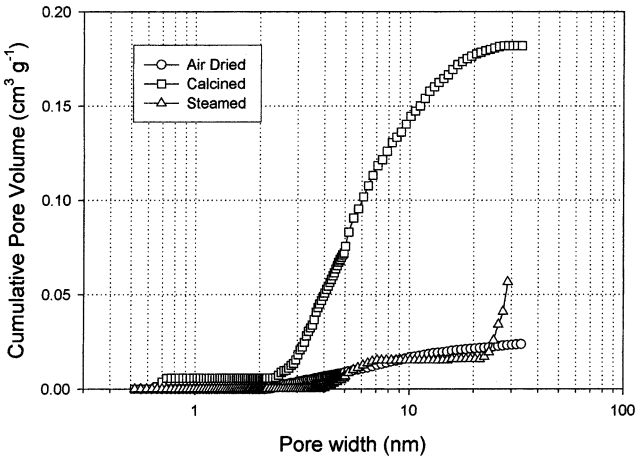

Figure 8. Cumulative pore volume distribution data obtained by fitting the DFT model to the sorption isotherms.

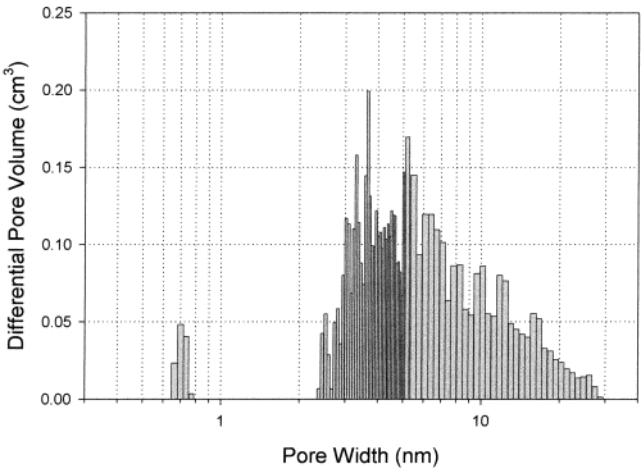

Figure 9. Differential pore volume distribution obtained by fitting the DFT model to the calcined HT sorption isotherm.

Table 3. Surface Area and Pore Volume Results from Nitrogen Porosimetry Data for the Steamed HT Sample[a]

method	micro. surface area (m^2/g)	total surface area (m^2/g)	micro. pore volume (cm^3/g)	pore volume (33.4 nm) (cm^3/g)
DFT	4	87	0.0016	0.10
BET		104		
Langmuir		105		
BJH		91		0.14.

[a] Total PV measured at p/Po ~0.995 = 0.32.

for the mesoporous solid under study the Langmuir, BET, and the BJH methods yield surface area values that do not deviate greatly from DFT results (Tables 1−3). However, only the DFT method allows us to extract from adsorption data a much more complete description of a porous material than traditional methods; see Figures 7−9.

NMR Results. The comparison in Figure 10 of ^{13}C CP NMR spectra of reference sodium acetate and air-dried (at 25 °C) HT crystals clearly show that the HT under study contains the expected charge-compensating acetate anions. The corresponding ^{27}Al NMR spectra of the same HT sample before and after thermal treatments are shown in Figure 11. As anticipated, the spectrum of the air-dried HT exhibits a single resonance (near 9.7 ppm) representing octahedrally coordinated

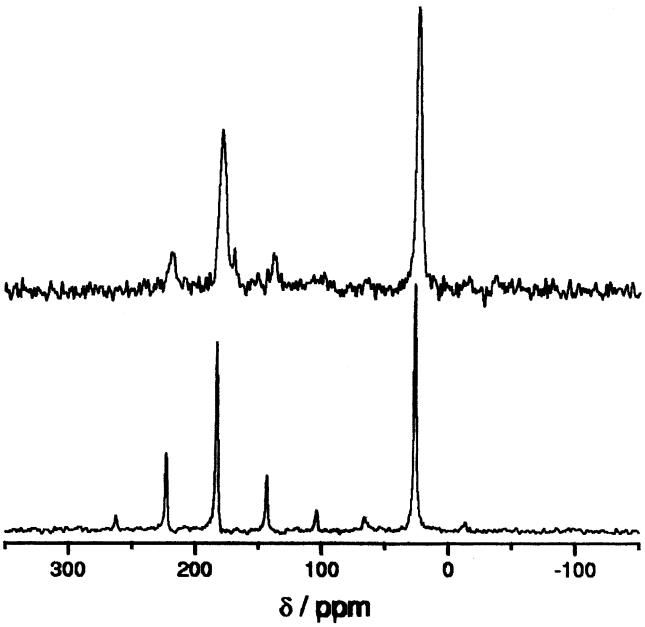

Figure 10. ^{13}C NMR spectra of reference sodium acetate (bottom) and of HT crystals air-dried at 25 °C (top).

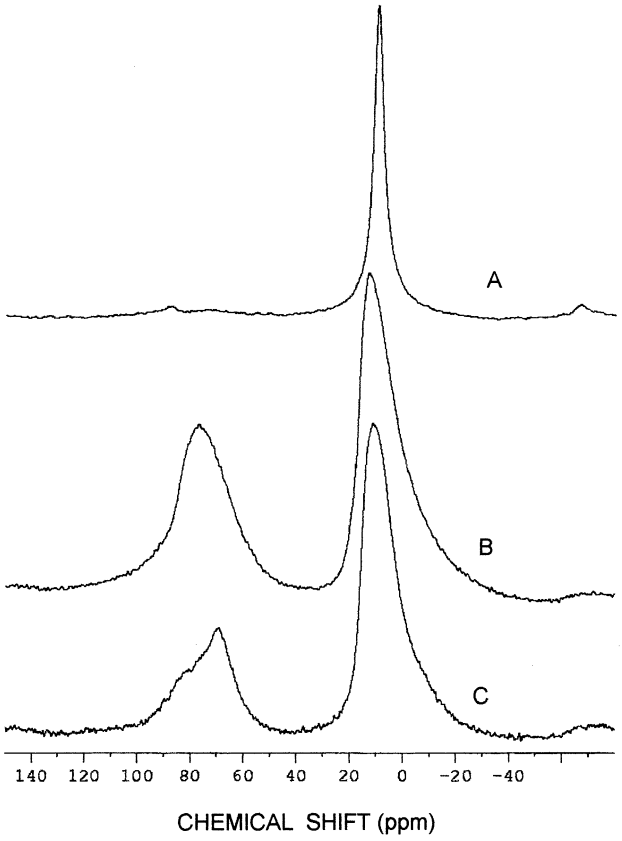

Figure 11. ^{27}Al MAS NMR spectra of HT samples after (A) air drying at 25 °C, (B) calcination at 500 °C, and (C) steam aging at 760 °C with 100% steam.

framework Al(VI) species, Figure 11A. On calcination at 500 °C in air, the stacks of brucite layers that form the HT lattice exfoliate and form a "house of cards" structure containing both Al(VI) and tetrahedrally coordinated Al(IV) species represented by resonances at 13.0 and 76.8 ppm respectively (Figure 11B). After steam-aging, the Al(VI) resonance shifts to 11.4 ppm, and the relative intensity of the Al(IV) resonance

Table 4. SO_2 Chemisorption Data at 30 °C (p = 0.2 Torr)

sample	μmol SO_2/g V_T	V_r	V_{Irr}	initial heat kJ/mol	integral heat J/g
HT, 25 °C	151	18	133	152	13.5
HT, 500 °C	981	92	889	190	141.0
HT, 500 °C[a]	689	64	625	199	109.0
HT, steamed	272	33	239	198	37.0

[a] Chemisorption at 80 °C.

Table 5. Site Population Distribution (in μmol SO_2/g) at 30 °C

sample	basic site strength in kJ/mol <100	100−120	120−150	150−200
HT, 25 °C	85	17	40	9
HT, 500 °C	155	45	251	530
HT, 500 °C[a]	76	54	84	475
HT, steamed	62	14	42	154

[a] Chemisorption at 80 °C.

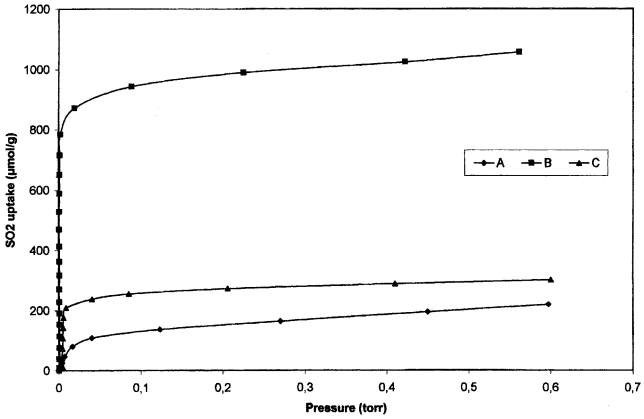

Figure 12. SO_2 sorption isotherms for HT samples after (A) air drying at 25 °C, (B) calcination at 500 °C, and (C) steam aging at 760 °C with 100% steam.

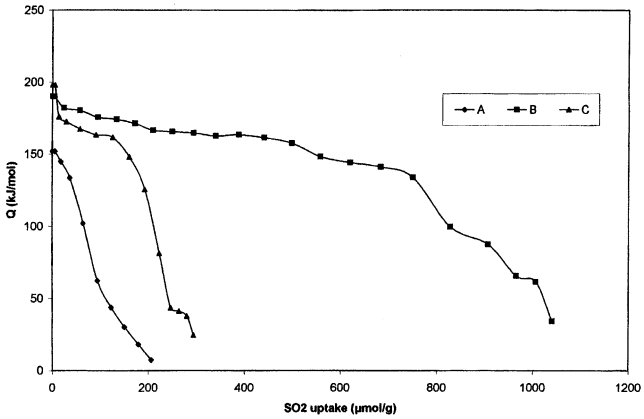

Figure 13. Differential heats profiles for HT samples after: A) Air drying at 25 °C, B) Calcination at 500 °C and C) Steam aging at 760 °C with 100% steam.

broadens, decreases in intensity, and shifts to 69.1 ppm with a shoulder near 79.3 ppm representing changes in the Al(IV) environment, resulting from spinel formation (Figure 11C).

Microcalorimetry Results. Adsorption microcalorimetry results with SO_2 as the probe molecules are reported in Tables 4 and 5 and in Figures 12 and 13. Chemisorption isotherms are in Figure 12. Not shown are secondary sorption isotherms, that is, sorption isotherms for samples after adsorption and degassing in a vacuum at 30 °C. By subtracting the adsorbed volume of the secondary isotherms (V_r) from that of the primary isotherms (V_T) at the same equilibrium pressure (p = 0.2 Torr), it is possible to obtain V_{Irr}, the volume of irreversibly chemisorbed SO_2. This value is believed to correlate with the presence of strong basic sites.[22−24] In Table 4, initial heats have been associated with the strength of the strongest adsorption sites present. On the other hand, integral heats represent the total heat of SO_2 adsorption evolved at p = 0.2 Torr and are therefore associated with the solid's density of basic sites.[23−24] At 30 °C the interlamellar space of the hydrotalcite structure is occupied by acetate anions and sites for SO_2 chemisorption are not available, thus explaining the low basic sites density and strength exhibited by this material; see Tables 4 and 5 and the differential heat curve in Figure 13. On calcination at 500 °C/2 h in air, the brucite layers that form the hydrotalcite crystals exfoliate forming a mesoporous house of cards structure available to SO_2 chemisorption. At 30 °C, the strength of the strongest basic adsorption sites in the calcined material is high, near 190 kJ/mo, and contains a large (530 μmol SO_2/g) population of basic sites with strength near 170 kJ/mol; see Figure 13. If the SO_2 saturated sample is exposed to hydrogen at 500 °C overnight and then reexposed to SO_2 in the microcalorimeter cell, the total amount of SO_2 sorbed decreased to 643 μmol SO_2/g from 981 μmol SO_2/g, indicating that only ∼66% of the original basic sites were regenerated. Specifically, sites with strength greater than 170 kJ/mol irreversibly sorb SO_2 at the above-mentioned conditions.

To compare the present results with those obtained with other solid-bases, the SO_2 chemisorption temperature was raised to 80 °C from 30 °C. Results in Tables 4 and 5 show the anticipated decrease in SO_2 sorption capacity at the higher temperature. At 80 °C, the initial heat of SO_2 chemisorption (199 kJ/mol) is 5 kJ/mol greater than the one reported for alumina but lower than the one (215 kJ/mol) measured on magnesia.[23] Thus, the calcined HT with 254 m^2/g surface area and 0.33 cm^3/g pore volume (at p/Po ∼0.995) is a solid base in which the strength of the strongest basic sites is greater than the one found in TiO_2, Sn/TiO_2, SnO_2, Ga_2O_3, Ga/Al_2O_3,[25,26] and NaY.[27] After steaming, the strength of the strongest sites is retained. However, the steam-aged material suffers a drastic reduction in basic sites density resulting from the collapse of the solid's porous structure and the formation of an $MgAl_2O_4$−MgO mixture; see Tables 3 and 4.

Summary and Conclusions

The hydrotalcite-like material described in this paper are particles formed by the long-range stacking of

(22) Auroux, A. In *Catalyst Characterization: Physical Techniques for Solid Materials*; Imelik, B., Vedrine, J. C., Eds.; Plenum Press, New York, 1994; Ch. 22.
(23) Auroux, A. *Top. Catal.* **1997**, *4*, 71−89.
(24) Gervasini, A.; Fenyvesi, J.; Auroux, A. *Langmuir* **1996**, *12*, 5356−5364.
(25) Gergely, B.; Redey, A.; Guimon, C.; Gervasini, A.; Auroux, A. J. *Ther. Anal. Cal.* **1999**, *56*, 1233−1241.
(26) Gergely, B.; Auroux, A. *Res. Chem. Intermed.* **1999**, *25*, 1, 13−24.
(27) Auroux, A.; Artizzu, P.; Ferino, I.; Monaci, R.; Rombi, E.; Solinas, V. *Microporous Mater.* **1997**, *11*, 117−126.

brucite layers in which the positive interlamellar charge, resulting from the isomorphous substitution of Mg with Al atoms, is compensated by acetate anions. The presence of acetate anions has been confirmed by ^{13}C CP NMR carbon results. Moreover,[27] Al NMR spectra indicate that only Al(VI) is present, while chemical analysis reports an Al/[CH_3COO] molar ratio of 1.02, lending support to the proposition that the layer net positive charge is indeed compensated by acetate anions.

The decomposition at 500 °C in air of interlamellar charge-compensating acetate anions causes the delamination (exfoliation) of the stacks of brucite layers and the formation of a mesoporous house-of-cards structure[32] with DFT surface area and pore volume of 254 m^2/g and 0.18 cm^3/g, respectively. This mesoporous solid behaves like a solid-base sorbing 689 μmol SO_2/g at 80 °C and 981 μmol SO_2/g at 30 °C. The strength (199 kJ/mol) of its strongest basic sites is intermediate to those of alumina and magnesia. When the calcined HT is exposed to steam at 760 °C, the mesoporous house-of-cards structure collapses forming an MgO and Al spinel mixture; the solid's DFT SA is reduced to 87 m^2/g from 254 m^2/g and loses most of its sorption capacity for SO_2. Thus, after recirculating in a fluid cracking unit, any LDH material initially present in FCC compositions[7] will convert to a MgO and Al-spinel mixture; that is, to compounds whose reactivity with sulfur oxides has long been recognized.[28,29] Microcalorimetry experiments reported in this paper show that the strength of the strongest basic sites is less than 200 kJ/mol. Sulfite formation is exothermic (ΔH of (($MgSO_3$) = −1009.6 kJ/mol) and it is unlikely that the aforementioned initial heats are related to this compound generation.

To elucidate the porous structure of layered materials a method based on molecular scale statistical thermodynamics is needed. The DFT provides such a method, and allows us to extract from adsorption data a much more complete description of the porous structure of a material than traditional methods.[31] In general, traditional methods of nitrogen porosimetry data representation yield surface area values that differ from actual areas in a manner that depends on the solid's pore structure, and when pore widths approach molecular dimensions the differences can be very large.[19−21] Only in the case of solids that do not contain significant amounts of micropores, such as the solid studied in this paper, do DFT methods yield surface area values that do not markedly deviate from Langmuir, BET, and BJH results.

Acknowledgment. Initially this work has been supported in part by NATO collaborative grant CRG-971497 to M.L.O. and H.E. Special thanks to Dr. B. Bonnetot for providing XRD results.

CM030105B

(28) Hirschberg, E. H.; Bertolacini, R. J. In *Fluid Catalytic Cracking: Role in Modern Refining*; Occelli, M. L., Ed.; ACS Symposium Series; American Chemical Society: Washington, DC, 1988; vol. 375, pp 114−145.

(29) Magnabosco, L. M.; Demmel, E. J. In *Fluid Catalytic Cracking III: Materials and Processes*; Occelli, M. L., O'Connor, P., Eds.; ACS Symposium Series; American Chemical Society: Washington, DC, 1994; vol. 571, pp 303−321.

(30) Rheaume, L.; Ritter, R. E. In *Fluid Catalytic Cracking: Role in Modern Refining*; Occelli, M. L., Ed.; ACS Symposium Series; American Chemical Society: Washington, DC, 1988; vol. 375, pp 146−161.

(31) Olivier, J. P.; Occelli, M. L. *J. Phys. Chem.* **2001**, *105* (3), 623−629.

(32) van Holpen, H. *An Introduction to Clay Colloidal Chemistry*; Wiley-Interscience: New York, 1977.